Chinese Physics Letters **42**, 053705 (2025) **Express Letter**

# Quantum Simulation of Two-Dimensional U(1) Gauge Theory in Rydberg and Rydberg-Dressed Atom Arrays

Zheng Zhou(周正)[2,3,4], Zheng Yan(严正)[5,6], Changle Liu(刘长乐)[1,7*], Yan Chen(陈焱)[2,8], and Xue-Feng Zhang(张学锋)[7,9]

[1]*School of Physics and Mechatronic Engineering, Guizhou Minzu University, Guiyang 550025, China*
[2]*Department of Physics and State Key Laboratory of Surface Physics, Fudan University, Shanghai 200438, China*
[3]*Perimeter Institute for Theoretical Physics, Waterloo, Ontario N2L 2Y5, Canada*
[4]*Department of Physics and Astronomy, University of Waterloo, Waterloo, Ontario, Canada N2L 3G1*
[5]*Department of Physics, School of Science and Research Center for Industries of the Future, Westlake University, Hangzhou 310030, China*
[6]*Institute of Natural Sciences, Westlake Institute for Advanced Study, Hangzhou 310024, China*
[7]*Department of Physics and Chongqing Key Laboratory for Strongly Coupled Physics, Chongqing University, Chongqing 401331, China*
[8]*Collaborative Innovation Center of Advanced Microstructures, Nanjing 210093, China*
[9]*Center of Quantum Materials and Devices, Chongqing University, Chongqing 401331, China*

(Received 3 April 2025; accepted manuscript online 22 April 2025)

Simulating U(1) quantum gauge theories with spatial dimensions greater than one is of great physical significance. Here we propose a simple realization of U(1) gauge theory with Rydberg and Rydberg-dressed atom arrays. Within the experimentally accessible range, we find that the various aspects of the U(1) gauge theory can be well simulated, such as the emergence of topological sectors, incommensurability, and the Rokhsar–Kivelson point that hosts deconfined charge excitations and degenerate topological sectors. Our proposal is promising to implement experimentally and exhibits pronounced quantum dynamics.

DOI: 10.1088/0256-307X/42/5/053705 CSTR: 32039.14.0256-307X.42.5.053705

*Introduction.* Quantum simulations based on programmable Rydberg atom arrays have recently emerged as a powerful platform to explore exotic many-body physics. Rydberg simulators allow flexible design of lattice geometry,[1,2] and high tunability of interaction strength far beyond condensed matter experiments.[3,4] A key element of quantum many-body simulations in Rydberg arrays is the Rydberg blockade mechanism, i.e., the van der Waals interactions strongly suppress the double occupancy of atomic Rydberg excitations within a certain blockade radius $R_c$.[5–7] In particular, the Rydberg blockade can lead to low-energy local constraints, which is an essential ingredient to realize lattice gauge theories (LGT),[8,9] a host of exotic phenomena such as quantum spin liquids,[10–12] fractionalized excitations with Abelian and non-Abelian statistics.[13,14] Very recently, significant progress has been made in realizing two-dimensional $\mathbb{Z}_2$ LGT.[15–19] In comparison, U(1) LGT involves more exotic phenomena like a large number of topological sectors,[8,20] incommensurability,[21–23] and deconfined quantum criticality.[20] Moreover, it sheds light on simulating more complex gauge fields in high-energy physics.[24,25] Recently, the one-dimensional U(1) LGT has been successfully simulated in Rydberg platforms.[26–30] Nevertheless, its implementation in higher dimensions involves complicated theoretical proposals,[31–35] and had not been achieved until recently.

One natural implementation of U(1) LGT is the quantum dimer model (QDM) on the honeycomb lattice which can be mapped to the antiferromagnetic transverse field Ising model (TFIM) on triangular lattice.[20,23,36–42] However, previous experiments simulating TFIM on Rydberg arrays[43] did not exhibit clear features of the U(1) gauge field. The physics of the 'order-by-disorder' (OBD)[44–48] region with possible gauge structures is still in the midst of interplay between intertwined interactions.

In this Letter, we propose a simple realization of U(1) LGT in Rydberg atom arrays with dressing technique.[49–52] We analyze the effective Hamiltonian with large-scale quantum Monte Carlo simulations. The softened repulsive interactions between Rydberg-dressed atoms provide various aspects of U(1) LGT, including emergent topological sectors, incommensurability, and the Rokhsar–Kivelson (RK) point that hosts deconfined criticality. Our work demonstrates that the mystery of the OBD region can be uncovered by dressing Rydberg atoms, and many characteristic properties of the U(1) LGT could be experimentally observed.

*Model of Rydberg-Dressed Atoms.* We consider that neutral atoms are arranged on a triangular lattice array.[43] At low energies, each atom is regarded as a two-level system where $|\downarrow\rangle$ is the atomic ground state and $|\uparrow\rangle$ is

*Corresponding author. Email: liuchangle89@gmail.com
© 2025 Chinese Physical Society and IOP Publishing Ltd. All rights, including for text and data mining, AI training, and similar technologies, are reserved.

the excited Rydberg state dressed with another hyperfine level.[49,52] The system is described by the following Hamiltonian

$$H = \sum_i \Big[ -\frac{\Omega}{2}(|\uparrow\rangle\langle\downarrow|_i + |\downarrow\rangle\langle\uparrow|_i) - \delta|\uparrow\rangle\langle\uparrow|_i \Big] + \sum_{ij} U_{ij}|\uparrow\rangle\langle\uparrow|_i \otimes |\uparrow\rangle\langle\uparrow|_j, \quad (1)$$

where $\Omega$ is the microwave Raman–Rabi frequency, $\delta$ is the detuning, and $U_{ij}$ is the repulsive interaction between Rydberg-dressed states. For undressed systems, the interactions are of the van der Waals type $U_{ij} = c_6/r_{ij}^6$. Upon dressing, the interaction profile becomes softer, with slower decays at short distances but the long-distance behavior stays the same.[49,51,52] As will be discussed later, the U(1) gauge mapping requires the nearest-neighbor (NN) coupling $U_1$ to be dominant, so we only focus on small $|\Omega|/U_1$ case. Meanwhile, the dressing technique renders the ratio between second- and third-NN interactions $U_2/U_3$ tunable, so that rich phenomena of the U(1) gauge field can emerge.

Another requirement of the U(1) LGT is the half-filling of Rydberg-dressed states, which can be achieved by tuning the chemical potential $\delta$. At $\delta = \frac{1}{2}\sum_{j\neq i} U_{ij}$, the Hamiltonian exhibits an additional $\mathbb{Z}_2$-symmetry $\mathscr{P}$ that exchanges the Rydberg-dressed state and the ground state $\mathscr{P}|\uparrow\rangle_i = |\downarrow\rangle_i$, $\mathscr{P}|\downarrow\rangle_i = |\uparrow\rangle_i$, so that the half-filling condition is fulfillled.

*Phase Diagram.* We numerically investigate the model Eq. (1) with large-scale quantum Monte Carlo simulations.[53–55] As the interaction is negligible at long distances, we truncate the interaction at the third-NN and study the phase diagram on the $U_2$-$U_3$ plane. The simulations are performed on $L \times L$ lattices with periodic boundary conditions at a temperature $T = L^{-2}U_1$. Most of our simulations take $L = 24, 36$, and in the finite-size scaling we take $L$ from 12 to 36, as shown in Supplementary Material (SM).

We find a rich quantum phase diagram as shown in Fig. 1(a). The clock and stripe orders are stabilized in the upper-left and lower-right regions in the phase diagram, respectively. The clock and stripe phases are separated by a first-order line at small $U_2$ values, and a fan-shaped intermediate region at larger $U_2$. The first-order line and the intermediate region terminate at a multicritical point. Through finite-size scaling, we determine its position in the thermodynamic limit $U_{2c}/\Omega = 0.547(5)$ and $U_{3c}/\Omega = 0.215(3)$.

The essential features of the phase diagram are achievable with experimentally relevant parameters [Figs. 1(a)–1(c)]. Here we employ an $^{87}$Rb atom array that has already been realized in the experiment,[43] and the phase diagram is shown in Fig. 1(b). To access a more extended region of the phase diagram Fig. 1(a), we perform Rydberg dressing, where the Rydberg-dressed state $|\uparrow\rangle$ is prepared by coupling the hyperfine state $|g\rangle = |5S_{1/2}, F = 2, m_F = 2\rangle$ and Rydberg state $|r\rangle = |53S_{1/2}, m_J = 1/2\rangle$ via a two-photon process.[56] The corresponding Rabi frequency $\Omega_L$ and detuning $\delta_L$ can be used to tune the

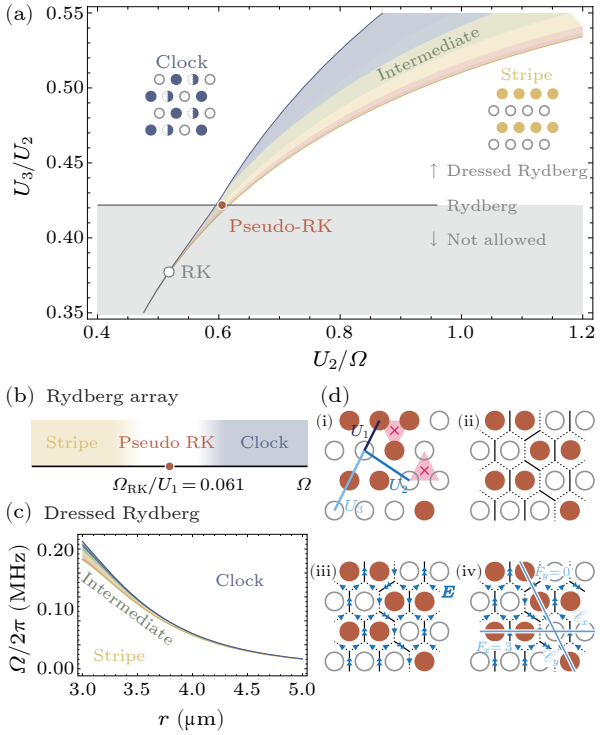


**Fig. 1.** Phase diagram of the model at half filling. (a) phase diagram on the $U_3/U_2$ plane; the dark gray line denotes the parameters accessed by the undressed Rydberg array and is further illustrated in (b); the unshaded region denotes the accessible region for Rydberg-dressed arrays. The data are simulated with lattice length $L = 24$ and $\Omega/U_1 = 0.2$. (c) Phase diagram with Rydberg-dressed settings; Here we take the experimental parameters from Ref. [43] with laser Rabi frequency $\Omega_L/2\pi = 4.3$ MHz and detuning $\delta_L/2\pi = 1.3$ MHz and $c_6/2\pi = 42729.4$ MHz·μm$^6$. (d) Illustration of the emergent U(1) gauge structure: (i) Interactions and the 'triangle-rule' constraint. Constraint-violating triangles are marked shaded with crossings; (ii) Mapping of atom configurations to fully-packed dimers; (iii) charge-free gauge field; and (iv) Emergent topological sectors.

soft-core potential between Rydberg-dressed atoms.[52] Meanwhile, one can choose another hyperfine level $|\downarrow\rangle = |5S_{1/2}, F = 1, m_F = 1\rangle$ as the ground state. The experimental phase diagram is shown in Fig. 1(c) and more details are discussed in SM.

*Emergent* U(1) *Gauge Field and Topological Sectors.* The structure of the phase diagram resembles that of the QDM on the honeycomb lattice, which is described by a U(1) LGT. To better understand the phase diagram, we start with the limit where $U_1$ is the dominant energy scale $U_1 \gg |\Omega|, |U_2|, |U_3|$. At half Rydberg filling, the Hamiltonian can be recast in the following form

$$H_{U_1} = \frac{U_1}{2}\sum_{\triangle}\Big(\sum_{i\in\triangle}|\uparrow\rangle_i\langle\uparrow| - \frac{3}{2}\Big)^2 + \text{const.} \quad (2)$$

It is clear that the ground state must satisfy a local constraint that either one or two occupations of Rydberg-dressed states within each unit triangle are allowed, while zero or three occupations are blockaded [panel (i) in Fig. 1(d)]. Such local constraint at half-filling gives rise to extensive ground-state degeneracy. This local constraint

within each triangle serves as the key ingredient of the emergent U(1) gauge field: we define the emergent electric field on the (oriented) link of the dual honeycomb lattice. The value of the electric field (from A to B sublattice) is assigned 2 if the triangular lattice bond crossing this link is frustrated, and is assigned $-1$ otherwise. Here we define a bond to be 'frustrated' if the two sites connected to this bond are occupied by the same states. Then this local constraint dictates that each unit triangle consists of one and only one frustrated bond, which translates to the charge-free condition of the U(1) gauge field at each dual vertex $\boldsymbol{v}$ [see panel (iii) in Fig. 1(d)]:

$$Q_{\boldsymbol{v}} \equiv (\mathrm{div}\, \boldsymbol{E})_{\boldsymbol{v}} = 0. \tag{3}$$

Note that this electric field configuration is equivalent to fully-packed dimers, by assigning each $\boldsymbol{E} = 2$ link with one dimer and the $\boldsymbol{E} = -1$ link with no dimer [panel (ii) in Fig. 1(d)]. We also note that as long as the local constraints are imposed by a sufficiently large $U_1$, its value no longer affects the physics of the system.

A direct consequence of the U(1) gauge structure is the emergence of topological sectors, which can be defined as follows.[38] For the two cuts $\mathscr{C}_x$ and $\mathscr{C}_y$ throughout the lattice [illustrated in panel (iv) of Fig. 1(d)], the corresponding electric fluxes that penetrate through these cuts are conserved quantities upon local fluctuations. Therefore, the low-energy Hilbert space can be divided into different topological sectors labeled by flux quantum numbers $(F_x, F_y)$. For the ground states, one of the fluxes is zero. Without loss of generality, we set $F_y = 0$ and use the flux density $f \equiv F_x/L_x$ to label topological sectors.

The emergent U(1) gauge structure in the large $U_1$ limit is robust against local perturbations such as $U_2$, $U_3$, and $\Omega$. As illustrated in Fig. 1(a), various density orders at different topological sectors are stabilized as the ground states in the phase diagram. These density wave orders can also be characterized by the ordering wave vectors in the Rydberg structure factor:

$$\mathscr{S}(\boldsymbol{Q}) = \frac{1}{N}\sum_{ij}\left\langle\left(n_i - \frac{1}{2}\right)\left(n_j - \frac{1}{2}\right)\right\rangle \mathrm{e}^{\mathrm{i}\boldsymbol{Q}\cdot(\boldsymbol{r}_i - \boldsymbol{r}_j)}, \tag{4}$$

where $n_i = |\uparrow\rangle_i\langle\uparrow|$ is the occupancy of the Rydberg-dressed atom at site $i$. The flux densities $f$, real-space configurations, and the Rydberg structure factors of each density order are illustrated in Fig. 2.

The three-sublattice 'clock' state has the ordering wave vector at the $K$ point and lives within the $f = 0$ sector. The 'clock' state is named after the six-fold clock anisotropy of the order parameter, as clearly illustrated in the histogram [panel (i) in Fig. 3(b)]. The clock state is stabilized via the quantum OBD mechanism.[44–48] The two-sublattice 'stripe' state is ordered at the $M$ point with saturated flux density $f = 2$. In between the 'clock' and the 'stripe' state lives a fan of intermediate phases with $0 < f < 2$. The ordering wave vector $\boldsymbol{Q}$ is typically incommensurate between the $K$ and the $M$ point, and is related with $f$ by $\boldsymbol{Q} = (\pm\frac{(2-f)\pi}{3}, \pm\frac{2\pi}{\sqrt{3}})$ and equivalent wave vectors connected by lattice symmetry.

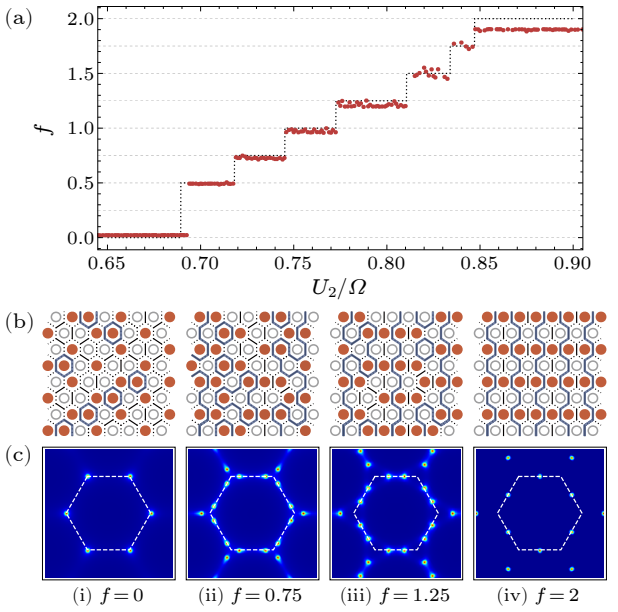


**Fig. 2.** Properties of each phase. (a) Flux density as a function of $U_2/\Omega$. (b) and (c) Real space patterns (b) and Rydberg structure factors (c) at different topological sectors. The data are simulated along the $U_3/U_2 = 0.5$ line with $L = 24$.

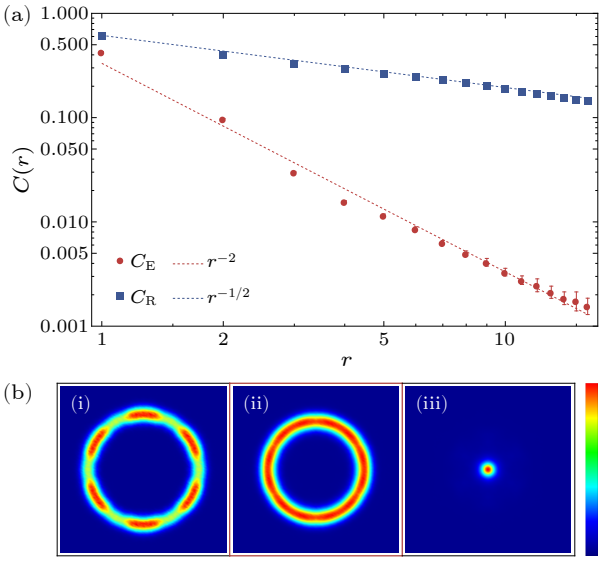


**Fig. 3.** (a) Electric field and Rydberg density correlators at the multicritical point measured with $L = 36$. Theoretical predicted behaviors are indicated by dashed lines. (b) Order parameter histogram within the clock phase $U_2/\Omega = 0.547$, $U_3/\Omega = 0.1$ (i); at the multicritical point $U_2/\Omega = 0.547$, $U_3/\Omega = 0.215$ (ii); and in the stripe phase $U_2/\Omega = 0.547$, $U_3/\Omega = 0.4$ (iii); measured with $L = 24$.

*Multicritical RK Point.* By comparing the overall phase diagram with the generic QDM on the honeycomb lattice,[21,38] we find that the most interesting aspect of our model is the correspondence between the multicritical point and the RK point of the QDM.[20,57] RK point is a quantum critical point separating clock and stripe states, and supports deconfined charge excitations right at the critical point.[20,37] It is described by (2 + 2)d quantum electrodynamics that supports quadratic gapless photons.[58,59] On the honeycomb lattice, the RK point

is multicritical with two relevant perturbations,[21,22,38] hence can be reached by tuning two system parameters. Here we present concrete evidence that this multicritical point indeed corresponds to the RK point.

A characteristic feature of the RK point is the exact ground state degeneracy among different topological sectors.[20,58] To verify, we measure the ground states with different sectors at the multicritical point with $L = 24$, and find vanishing energy difference $\sim 6 \times 10^{-4} L^2 \Delta$. The tiny difference is accounted by the marginally and dangerously irrelevant terms,[21,22] which do not vanish at finite system size (details in SM).

Further evidence of RK point is provided by checking the order parameter correlations. We first measure the electric field correlator $C_{\rm E}(\boldsymbol{R} - \boldsymbol{R}') = \langle \psi^*_{\rm E}(\boldsymbol{R}) \psi_{\rm E}(\boldsymbol{R}') \rangle$, where

$$\psi_{\rm E} = E_{\boldsymbol{b}_1} + E_{\boldsymbol{b}_2} {\rm e}^{-{\rm i}2\pi/3} + E_{\boldsymbol{b}_3} {\rm e}^{{\rm i}2\pi/3} \tag{5}$$

is the order parameter of the electric field. Here $E_{\boldsymbol{b}_i}$, $i = 1, 2, 3$ represent the electric field along three directions. At RK point, such correlator is predicted to follow the long-distance behavior $C_{\rm E}(\boldsymbol{R}) \sim |\boldsymbol{R}|^{-2}$,[60] and is clearly observed in our simulations [Fig. 3(a), red line]. We also measure the Rydberg density correlator $C_{\rm R}(\boldsymbol{R} - \boldsymbol{R}') = \langle \psi^*_{\rm R}(\boldsymbol{R}) \psi_{\rm R}(\boldsymbol{R}') \rangle$, where

$$\psi_{\rm R} = n_{\rm A} + n_{\rm B} {\rm e}^{{\rm i}2\pi/3} + n_{\rm C} {\rm e}^{-{\rm i}2\pi/3} \tag{6}$$

is the order parameter of the clock density-wave. The Rydberg correlator is predicted to satisfy $C_{\rm R}(\boldsymbol{R}) \sim |\boldsymbol{R}|^{-1/2}$, also consistent with our results [Fig. 3(a), blue line].

A hallmark of deconfined U(1) gauge field is the presence of emergent continuous symmetries, which can be examined in histograms of the order parameters. We measure the histograms of the clock order parameter $\psi_{\rm R}$ around the multicritical point, see Fig. 3(b). In the clock phase, $\psi_{\rm R}$ is pinned to six distinct values in the histogram, indicating relevance of instantons[21,58,61] [panel (i) in Fig. 3(b)]. For the stripe phase the histogram shrinks into a central peak [panel (iii) in Fig. 3(b)] indicating absence of three-sublattice ordering. At the multicritical point, we find that the U(1) symmetry emerges as a symmetric ring in the histogram [panel (ii) in Fig. 3(b)]. The right presence of the emergent U(1) symmetry at the multicritical point is consistent with the irrelevance of instantons and deconfinement of charges.[20,22,62] Considering that the local density profile of Rydberg-dressed states can be directly detected in experiments,[4] all the observables discussed above can be extracted.

*Excitations at the Multicritical Point.* Here we turn to the dynamical properties at the multicritical point. We measure the dynamical electric field and Rydberg density correlators:

$$\begin{aligned} G_{\rm E}(\boldsymbol{q}, \tau) &= \frac{1}{L^2} \sum_{\boldsymbol{R}, \boldsymbol{R}'} {\rm e}^{{\rm i}(\boldsymbol{R} - \boldsymbol{R}') \cdot \boldsymbol{q}} \langle E^y_{\boldsymbol{R}}(\tau) E^y_{\boldsymbol{R}'}(0) \rangle, \\ G_{\rm R}(\boldsymbol{q}, \tau) &= \frac{1}{L^2} \sum_{ij} {\rm e}^{{\rm i}(\boldsymbol{r}_i - \boldsymbol{r}_j) \cdot \boldsymbol{q}} \langle n_i(\tau) n_j(0) \rangle. \end{aligned} \tag{7}$$

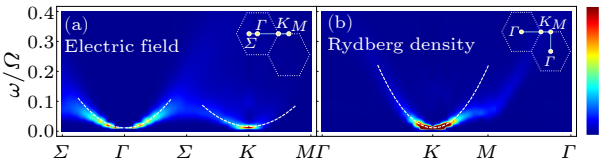


**Fig. 4.** (a) Electric field and (b) Rydberg density excitation spectra at the multicritical point. The data are simulated at the $f = 0$ topological sector with system size $L = 24$.

Here $E^y_{\boldsymbol{R}}$ represents the electric field originating from site $\boldsymbol{R}$ along the $y$-direction. The spectra are obtained from the imaginary time correlations via stochastic analytical continuation.[63–65] As widely discussed in the QDM, at RK point two gapless quadratic excitations present in the electric field spectra:[66,67] the 'resonon' around $\Gamma$ point that corresponds to the gauge photon, and the 'pi0n' around $K$ point due to the proximity to the three-sublattice ordered phase. These two quadratic excitations are indeed observed in our numerical spectra [Fig. 4(a)]. Further, the distinct curvatures of these two excitations exclude band folding and indicate their distinct physical nature.

For the Rydberg density correlators, we observe only one branch of quadratic excitation stemming from the $K$ point [Fig. 4(b)], with curvature different from the previous two. This excitation can be regarded as fractionalized 'pi0n' that transforms non-trivially under the symmetry $\mathscr{P}$. Hence we dub this new excitation 'pi0n*'.

*Advantages of Rydberg-Dressed Platform.* Our proposal has several advantages compared with previous ones realizing two-dimensional LGT. In our proposal, only one species of atom is required and the arrangement is the simple triangular lattice. Owing to the rapid development of Rydberg atom experiments, the Rydberg-dressed atom array on a triangular lattice is highly achievable in the near future. Moreover, our proposal overcomes an important issue on the lack of quantum dynamics in previous proposals. In LGT the quantum dynamics are contributed by the ring-exchange processes, which usually arise as high order perturbative terms and are thus strongly suppressed at low energies.[15–19,31–35,68,69] The suppressed quantum dynamics make the system glassy and thus hard to be simulated experimentally.[70] In contrast, in our scheme, the gauge dynamics is directly proportional to the first order of the Rabi-frequency $\Omega$, which can be significant and highly tunable. We believe that our system provides an ideal platform for exploring exotic quantum aspects of LGT.

*Discussions.* Simulating LGT in more than one dimension is of great interest and physical significance. Our proposal based on Rydberg-dressed atom arrays provides a simple and direct realization of the two-dimensional U(1) LGT. It also allows further investigation of broad aspects of U(1) LGT. Moreover, it provides an ideal platform to investigate topological excitations such as 'spinons' and 'topological strings'.[23,41,71] With rapid developments of the Rydberg platforms in recent years, various unconventional measurements such as snapshots and non-local correlation probes now become possible.

The most interesting region in the phase diagram locates at the boundary between the clock and stripe states,

which turns out to be most accessible in Rydberg-based experiments. For undressed Rydberg platforms, the experimentally accessible region is indicated by the thick black line in Fig. 1(a), which cuts through the intermediate region with negligible thickness. Such small thickness indicates that the relevant cubic anisotropy term is sufficiently small[22] so that the intermediate region lies sufficiently close to the celebrated RK point. As evidence, the energy difference among topological sectors is $\sim 1.1 \times 10^{-3} \Omega L^2$, still much less than the typical energy scale of this system. Hence we claim that the RK point can be simulated directly with conventional Rydberg experiments. With Rydberg-dressed atoms[50] one can further access an extended region of the phase diagram [marked unshaded in Fig. 1(a)] that includes the intermediate phases. This region also hosts interesting physics, such as incommensurability, Kasteleyn transition,[72–74] and even the 'Cantor deconfinement' of gauge field.[21,22] We expect that the interesting physics of this region will be unveiled with Rydberg-dressed atom arrays in future experiments.

*Acknowledgements.* We wish to thank Rong Yu, Hai-Zhou Lu, Yuan Wan, Yin-Chen He, Yue Yu, Yiming Wang, Jiucai Wang and Chun-Jiong Huang for their valuable discussions. X.-F. Zhang thank Heng Shen for his practical suggestions on the feasibility of the experiment proposals. C.L. thanks Rong Yu for hospitality inviting him to visit Renmin University of China where part of the work is done. This work is supported by the National Key Research and Development Program of China (Grant Nos. 2022YFA1404204 and 2022YFA1403700), the National Natural Science Foundation of China (Grant Nos. 12274086, 11534001 and 11925402). X.-F. Z. acknowledges funding from the National Science Foundation of China (Grant Nos. 12274046, 11874094, 12147102, and 12347101), Chongqing Natural Science Foundation (Grant No. CSTB2022NSCQ-JQX0018), the Fundamental Research Funds for the Central Universities (Grant No. 2021CDJZYJH-003), and Xiaomi Foundation/Xiaomi Young Talents Program. Z.Y. thanks the supports of the start-up funding of Westlake University. Z.Z. acknowledges support from the Natural Sciences and Engineering Research Council of Canada (NSERC) through Discovery Grants. Research at Perimeter Institute is supported in part by the Government of Canada through the Department of Innovation, Science and Industry Canada and by the Province of Ontario through the Ministry of Colleges and Universities.

# References

[1] Endres M, Bernien H, Keesling A, Levine H, Anschuetz E R, Krajenbrink A, Senko C, Vuletic V, Greiner M, and Lukin M D 2016 *Science* **354** 1024
[2] Barredo D, Lienhard V, de Léséleuc S, Lahaye T, and Browaeys A 2018 *Nature* **561** 79
[3] Bluvstein D, Omran A, Levine H, Keesling A, Semeghini G, Ebadi S, Wang T T, Michailidis A A, Maskara N, Ho W W, Choi S, Serbyn M, Greiner M, Vuletić V and Lukin M D 2021 *Science* **371** 1355
[4] Browaeys A and Lahaye T 2020 *Nat. Phys.* **16** 132
[5] Jaksch D, Cirac J I, Zoller P, Rolston S L, Côté R, and Lukin M D 2000 *Phys. Rev. Lett.* **85** 2208
[6] Lukin M D, Fleischhauer M, Cote R, Duan L M, Jaksch D, Cirac J I, and Zoller P 2001 *Phys. Rev. Lett.* **87** 037901
[7] Browaeys A, Barredo D, and Lahaye T 2016 *J. Phys. B* **49** 152001
[8] Kogut J B 1979 *Rev. Mod. Phys.* **51** 659
[9] Yan Z, Samajdar R, Wang Y C, Sachdev S, and Meng Z Y 2022 *Nat. Commun.* **13** 5799
[10] Balents L 2010 *Nature* **464** 199
[11] Savary L and Balents L 2016 *Rep. Prog. Phys.* **80** 016502
[12] Zhou Y, Kanoda K, and Ng T K 2017 *Rev. Mod. Phys.* **89** 025003
[13] Kitaev A 2006 *Ann. Phys.* **31** 2
[14] Grover T and Senthil T 2011 *Phys. Rev. Lett.* **107** 077203
[15] Verresen R, Lukin M D, and Vishwanath A 2021 *Phys. Rev. X* **11** 031005
[16] Tarabunga P S, Surace F M, Andreoni R, Angelone A, and Dalmonte M 2022 *Phys. Rev. Lett.* **129** 195301
[17] Samajdar R, Ho W W, Pichler H, Lukin M D, and Sachdev S 2021 *Proc. Natl. Acad. Sci.* **118** e2015785118
[18] Samajdar R, Joshi D G, Teng Y, and Sachdev S 2023 *Phys. Rev. Lett.* **130** 043601
[19] Semeghini G, Levine H, Keesling A, Ebadi S, Wang T T, Bluvstein D, Verresen R, Pichler H, Kalinowski M, Samajdar R *et al.* 2021 *Science* **374** 1242
[20] Moessner R and Raman K S 2011 *Quantum dimer models Introduction to Frustrated Magnetism* (Springer) p. 437
[21] Fradkin E, Huse D A, Moessner R, Oganesyan V, and Sondhi S L 2004 *Phys. Rev. B* **69** 224415
[22] Vishwanath A, Balents L, and Senthil T 2004 *Phys. Rev. B* **69** 224416
[23] Zhou Z, Liu C, Liu D X, Yan Z, Chen Y, and Zhang X F 2023 *SciPost Phys.* **14** 037
[24] Bauer C W, Davoudi Z, Balantekin A B, Bhattacharya T, Carena M, de Jong W A, Draper P, El-Khadra A, Gemelke N, Hanada M, Kharzeev D, Lamm H, Li Y Y, Liu J, Lukin M, Meurice Y, Monroe C, Nachman B, Pagano G, Preskill J, Rinaldi E, Roggero A, Santiago D I, Savage M J, Siddiqi I, Siopsis G, Van Zanten D, Wiebe N, Yamauchi Y, Yeter-Aydeniz K, and Zorzetti S 2023 *PRX Quantum* **4** 027001
[25] Tagliacozzo L, Celi A, Orland P, Mitchell M W, and Lewenstein M 2013 *Nat. Commun.* **4** 2615
[26] Zhou Z Y, Su G X, Halimeh J C, Ott R, Sun H, Hauke P, Yang B, Yuan Z S, Berges J, and Pan J W 2022 *Science* **377** 311
[27] Yang B, Sun H, Ott R, Wang H Y, Zache T V, Halimeh J C, Yuan Z S, Hauke P, and Pan J W 2020 *Nature* **587** 392
[28] Cheng Y, Liu S, Zheng W, Zhang P, and Zhai H 2022 *PRX Quantum* **3** 040317
[29] Martinez E A, Muschik C A, Schindler P, Nigg D, Erhard A, Heyl M, Hauke P, Dalmonte M, Monz T, Zoller P, and Blatt R 2016 *Nature* **534** 516
[30] Surace F M, Mazza P P, Giudici G, Lerose A, Gambassi A, and Dalmonte M 2020 *Phys. Rev. X* **10** 021041
[31] Celi A, Vermersch B, Viyuela O, Pichler H, Lukin M D, and Zoller P 2020 *Phys. Rev. X* **10** 021057
[32] Tagliacozzo L, Celi A, Zamora A, and Lewenstein M 2013 *Ann. Phys.* **330** 160
[33] Glaetzle A W, Dalmonte M, Nath R, Rousochatzakis I, Moessner R, and Zoller P 2014 *Phys. Rev. X* **4** 041037
[34] Osborne J, McCulloch I P, Yang B, Hauke P, and Halimeh J C 2022 arXiv:2211.01380 [cond-mat.quant-gas]
[35] Zohar E, Cirac J I, and Reznik B 2013 *Phys. Rev. Lett.* **110** 055302
[36] Fradkin E and Kivelson S 1990 *Mod. Phys. Lett. B* **04** 225
[37] Moessner R, Sondhi S L, and Chandra P 2001 *Phys. Rev. B* **64** 144416
[38] Schlittler T, Barthel T, Misguich G, Vidal J, and Mosseri R 2015 *Phys. Rev. Lett.* **115** 217202

[39] Yan Z, Zhou Z, Syljuåsen O F, Zhang J, Yuan T, Lou J, and Chen Y 2021 *Phys. Rev. B* **103** 094421
[40] Ran X, Yan Z, Wang Y C, Rong J, Qi Y, and Meng Z Y 2023 *Phys. Rev. B* **107** 125134
[41] Zhou Z, Liu C, Yan Z, Chen Y, and Zhang X F 2022 *npj Quantum Mater.* **7** 60
[42] Yan Z, Zhou Z, Zhou Y H, Wang Y C, Qiu X, Meng Z Y, and Zhang X F 2023 *npj Quantum Inf.* **9** 89
[43] Scholl P, Schuler M, Williams H J, Eberharter A A, Barredo D, Schymik K N, Lienhard V, Henry L P, Lang T C, Lahaye T *et al.* 2021 *Nature* **595** 233
[44] Villain J, Bidaux R, Carton J P, and Conte R 1980 *J. Phys. France* **41** 1263
[45] Moessner R, Sondhi S L, and Chandra P 2000 *Phys. Rev. Lett.* **84** 4457
[46] Moessner R and Sondhi S L 2001 *Phys. Rev. B* **63** 224401
[47] Isakov S V and Moessner R 2003 *Phys. Rev. B* **68** 104409
[48] Koziol J, Fey S, Kapfer S C, and Schmidt K P 2019 *Phys. Rev. B* **100** 144411
[49] Jau Y Y, Hankin A M, Keating T, Deutsch I H, and Biedermann G W 2016 *Nat. Phys.* **12** 71
[50] Graham T M, Song Y, Scott J, Poole C, Phuttitarn L, Jooya K, Eichler P, Jiang X, Marra A, Grinkemeyer B, Kwon M, Ebert M, Cherek J, Lichtman M T, Gillette M, Gilbert J, Bowman D, Ballance T, Campbell C, Dahl E D, Crawford O, Blunt N S, Rogers B, Noel T, and Saffman M 2022 *Nature* **604** 457
[51] Johnson J E and Rolston S L 2010 *Phys. Rev. A* **82** 033412
[52] Zeiher J, van Bijnen R, Schauß P, Hild S, Choi J Y, Pohl T, Bloch I, and Gross C 2016 *Nature Physics* **12** 1095
[53] Sandvik A W 1997 *Phys. Rev. B* **56** 11678
[54] Sandvik A W 2003 *Phys. Rev. E* **68** 056701
[55] Avella A and Mancini F 2013 *Strongly correlated systems: numerical methods* (Springer, Berlin) **176**
[56] Evered S J, Bluvstein D, Kalinowski M, Ebadi S, Manovitz T, Zhou H, Li S H, Geim A A, Wang T T, Maskara N, Levine H, Semeghini G, Greiner M, Vuletić V, and Lukin M D 2023 *Nature* **622** 268
[57] Rokhsar D S and Kivelson S A 1988 *Phys. Rev. Lett.* **61** 2376
[58] Henley C L 1997 *J. Stat. Phys.* **89** 483
[59] Moessner R, Sondhi S L, and Fradkin E 2001 *Phys. Rev. B* **65** 024504
[60] Stephenson J 1966 *J. Math. Phys.* **7** 1123
[61] Polyakov A M 1977 *Nucl. Phys. B* **120** 429
[62] Senthil T, Vishwanath A, Balents L, Sachdev S, and Fisher M P A 2004 *Science* **303** 1490
[63] Sandvik A W 1998 *Phys. Rev. B* **57** 10287
[64] Shao H, Qin Y Q, Capponi S, Chesi S, Meng Z Y, and Sandvik A W 2017 *Phys. Rev. X* **7** 041072
[65] Sandvik A W 2016 *Phys. Rev. E* **94** 063308
[66] Läuchli A M, Capponi S, and Assaad F F 2008 *J. Stat. Mech.* **2008** P01010
[67] Moessner R and Sondhi S L 2003 *Phys. Rev. B* **68** 184512
[68] Hermele M, Fisher M P A, and Balents L 2004 *Phys. Rev. B* **69** 064404
[69] Savary L and Balents L 2017 *Phys. Rev. Lett.* **118** 087203
[70] Yan Z, Wang Y C, Samajdar R, Sachdev S, and Meng Z Y 2023 *Phys. Rev. Lett.* **130** 206501
[71] Wan Y and Tchernyshyov O 2012 *Phys. Rev. Lett.* **108** 247210
[72] Kasteleyn P W 1963 *J. Math. Phys.* **4** 287
[73] Moessner R and Sondhi S L 2003 *Phys. Rev. B* **68** 064411
[74] Powell S 2022 *Phys. Rev. B* **105** 064413